Available online at BCREC website: https://bcrec.id

Bulletin of Chemical Reaction Engineering & Catalysis, 16 (1) 2021, 97-110

Research Article

High Active Co/$Mg_{1-x}Ce_x^{3+}O$ Catalyst: Effects of Metal-Support Promoter Interactions on CO_2 Reforming of CH_4 Reaction

Faris A. J. Al-Doghachi[1,*], Diyar M. A. Murad[1], Huda S. Al-Niaeem[1], Salam H. H. Al-Jaberi[2], Surahim Mohamad[3], Yun Hin Taufiq-Yap[3,4,*]

[1]*Department of Chemistry, Faculty of Science, University of Basrah, 61004, Basrah, Iraq.*
[2]*Missan Health Department, Ministry of Health, Missan, Iraq.*
[3]*Catalysis Science and Technology Research Centre, Faculty of Science, University Putra Malaysia, 43400, UPM, Serdang, Selangor, Malaysia.*
[4]*Faculty of Science and Natural Resources, University Malaysia Sabah, 88400, Kota Kinabalu, Sabah, Malaysia.*

Received: 30th December 2020; Revised: 8th February 2021; Accepted: 8th February 2021; Available online: 25th February 2021; Published regularly: March 2021

Abstract

Co/$Mg_{1-x}Ce^{3+}{}_xO$ (x = 0, 0.03, 0.07, 0.15; 1 wt% cobalt each) catalysts for the dry reforming of methane (DRM) reaction were prepared using the co-precipitation method with K_2CO_3 as precipitant. Characterization of the catalysts was achieved by X-ray diffraction (XRD), X-ray fluorescence spectroscopy (XRF), X-ray photoelectron spectroscopy (XPS), temperature programmed reduction (H_2-TPR), Brunauer–Emmett–Teller (BET), transmission electron microscopy (TEM), and thermal gravimetric analysis (TGA). The role of several reactant and catalyst concentrations, and reaction temperatures (700–900 °C) on the catalytic performance of the DRM reaction was measured in a tubular fixed-bed reactor under atmospheric pressure at various CH_4/CO_2 concentration ratios (1:1 to 2:1). Using X-ray diffraction, a surface area of 19.2 $m^2.g^{-1}$ was exhibited by the Co/$Mg_{0.85}Ce^{3+}{}_{0.15}O$ catalyst and MgO phase (average crystallite size of 61.4 nm) was detected on the surface of the catalyst. H_2 temperature programmed reaction revealed a reduction of CoO particles to metallic Co^0 phase. The catalytic stability of the Co/$Mg_{0.85}Ce^{3+}{}_{0.15}O$ catalyst was achieved for 200 h on-stream at 900 °C for the 1:1 CH_4:CO_2 ratio with an H_2/CO ratio of 1.0 and a CH_4, CO_2 conversions of 75% and 86%, respectively. In the present study, the conversion of CH_4 was improved (75%–84%) when conducting the experiment at a lower flow of oxygen (1.25%). Finally, the deposition of carbon on the spent catalysts was analyzed using TEM and Temperature programmed oxidation-mass spectroscopy (TPO-MS) following 200 h under an oxygen stream. Better anti-coking activity of the reduced catalyst was observed by both, TEM, and TPO-MS analysis.

Copyright © 2021 by Authors, Published by BCREC Group. This is an open access article under the CC BY-SA License (https://creativecommons.org/licenses/by-sa/4.0).

Keywords: Dry reforming of methane; MgO-Ce_2O_3 catalyst; Synthesis gas; H_2 production

How to Cite: F.A.J. Al-Doghachi, D.M.A. Murad, H.S. Al-Niaeem, S.H.H. Al-Jaberi, S. Mohamad, Y.H. Taufiq-Yap (2021). High Active Co/$Mg_{1-x}Ce_x^{3+}O$ Catalyst: Effects of Metal-Support Promoter Interactions on CO_2 Reforming of CH_4 Reaction. *Bulletin of Chemical Reaction Engineering & Catalysis*, 16(1), 97-110, (doi:10.9767/bcrec.16.1.9969.97-110)

Permalink/DOI: https://doi.org/10.9767/bcrec.16.1.9969.97-110

1. Introduction

The massive dependence on fossil fuels has substantially elevated the demand for energy. Consequently, the tremendous rise in the emission of some greenhouse gases in the atmosphere, particularly CO_2, along with the continuing economical and population growth has led to a critical change in the climate. To overcome

* Corresponding Author.
Email: farisj63@gmail.com (F.A.J. Al-Doghachi);
taufiq@upm.edu.my (Y.H. Taufiq-Yap)

these challenges, sustainable energy solutions are necessary. The production of biogas (CH_4 and CO_2) by the biomass digestion in the absence of oxygen (fermented wastes) has been utilized as a fuel for the production of power and heat. Biogas has also been used for industrial feedstock as a renewable carbon source in the syngas production (CO and H_2) through an environmental and economical friendly reaction [1,2]. One of the methods for this process is the dry reforming that requires intensive energy along with using CO_2 as an oxidant, as shown in Eq. (1).

$$CH_4 + CO_2 \rightarrow 2CO + 2H_2 \qquad \Delta G^0 = 256.7 - 0.28T \text{ kJ/mol} \tag{1}$$

Syngas is an important feedstock that can be converted effectively to fuel (gasoline, gasoil, gasoline, dimethyl ether (DME), and methanol) using the Fischer-Tropsch synthesis [3]. However, variations in the molar ratios of H_2/CO are essential to concur with the industrial syngas applications. For instance, an H_2/CO ratio of 2 is mandatory for the synthesis of methanol [4]; while that for DME synthesis is 1 under a one-step process [5]. Depending on the synthesized fuel, an H_2/CO ratio of 1-2 is required for the process of Fischer-Tropsch [6].

Reverse water-gas shift (RWGS) reaction (Eq. (2)) was found to influence the reaction's equilibrium during the syngas production from CH_4 and CO_2 (Eq. (1)) resulting in a low H_2/CO ratio.

$$CO_2 + H_2 \rightarrow CO + H_2O \qquad \Delta G^0 = 34.51 - 0.03T \text{ kJ/mol} \tag{2}$$

Other side reactions such as the decomposition of CH_4 (Eq. (3)) and Boudouard reaction (disproportionation reaction) (Eq. (4)) were also associated with dry reforming.

$$CH_4 \rightarrow C + 2H_2 \qquad \Delta G^0 = 89.53 - 0.11T \text{ kJ/mol} \tag{3}$$

$$2CO \rightarrow C + CO_2 \rightarrow CO_2 + C \qquad \Delta G^0 = -170.34 + 0.18T \text{ kJ/mol} \tag{4}$$

Zhang *et al*. [7] demonstrated a direct relation between the decomposition of CH_4 and CO disproportionation and the carbon deposition on the catalyst. Moreover, as the temperature of the reaction increased from 550 °C to 650 °C, the carbon deposition occurred more than the dry reforming of CH_4 (DRM). Thus, the careful selection of catalyst is crucial for preventing carbon formation and improving the DRM reaction [7]. Furthermore, the deposition of carbon can be reduced and even eliminated by supporting the metal in a metal oxide with strong basicity [8]. This finding results due to the chemical adsorption of the support that induces the catalyst to chemisorb CO_2 in the DRM in which CO_2 eventually forms CO by reacting with C (Eq. (5)).

$$CO_2 + C \rightarrow CO \qquad \Delta G^0 = 170.34 - 0.18T \text{ kJ/mol} \tag{5}$$

Due to their availability, and inexpensive cost, the use of nickel and cobalt has been highly recommended for the reforming process. However, a main disadvantage when using nickel or cobalt is the carbon formation that eventually deactivates the catalyst [9]. Accordingly, many studies have been conducted with the aim of improving the catalytic activity and stability of the cobalt and nickel catalysts in the reforming process [10]. The addition of strong Lewis base promoters (CaO or MgO) was found to deactivate the Ni-based catalysts. This can be improved by the chemisorption of CO_2 to lessen the coke deposition that forms CO by reacting with the deposited carbon [11]. A study by Hui Wang [12] revealed the dependence of the catalysts containing Co on the nature of the used support composite and showed that Co was only active when supported on Mg-Al-O_x composite support [12]. In addition, the preparation of Co-Ce/ZrO_2 catalysts by Paksoy *et al*. [13] revealed an increased stability when adding Ce, due to the minimization of the Co oxidation during the reaction of DRM. In the same study, no significant formation of carbon on the surface of the spent catalyst was observed along with no significant metal sintering. Also, the periodic redox of the catalysts was accelerated by the eminent transfer performance of Ce and the surface oxygen storage. A study by Casanovas *et al*. [14] on the various promoters modified Co-based catalysts demonstrated that in comparison to the other promoters, the selectivity and the catalytic performance of Na modified Co/ZnO catalysts was higher than the unmodified catalysts. Like wise, CaO and MgO (alkaline earth metal oxides) were studied for their potential as promoters modified Ni-based catalysts by Jang *et al*. [15]. Study findings revealed a higher stability and hindrance of carbon deposition by the MgO modified catalyst at an elevated reaction space velocity. The prevention of carbon deposition by the catalyst was due to the strong Lewis basicity on Mg modified catalyst, resulting in an outstanding CO_2 chemical adsorption, favorable for eliminating the deposition of carbon through CO disproportionation (Eq. (4)). In the same study, resistance to the deposition of carbon was observed more in the

Copyright © 2021, ISSN 1978-2993

MgO modified Co/Al_2O_3 catalyst as compared to the unmodified catalyst, indicating a better stability and hydrogen selectivity by the MgO modified Co/Al_2O_3 catalyst attributed to the characteristics of MgO [16].

The present study aimed at developing a stable catalyst that is highly active with strong selectivity and ability to reduce the deposition of carbon on the catalyst during DRM reaction. The method of co-precipitation included the precipitant K_2CO_3. In the study, 1% Co from cobalt acetylacetonate was impregnated into $MgO\text{-}Ce_2O_3$ to prepare $Co/Mg_{1-x}Ce_xO$ catalysts. The catalytic stability, effect of the conversion temperature and the CO_2 and CH_4 concentrations on the prepared catalysts were also investigated in the DRM. In addition, improvements in the CH_4 conversion when passing a stream of 1.25% O_2 gas in the process were also determined.

2. Materials and Methods

2.1 Materials

99.7% K_2CO_3, 99.0% $Ce(NO_3)_3.6H_2O$ and 99.0% $Mg(NO_3)_2.6H_2O$ were purchased from Merck Company, whereas, 99.0% $Co(C_5H_7O_2)_2 \cdot H_2O$ was obtained from Acros Organics.

2.2 Preparation of Catalysts

The promoter-supports $Mg_{1-x}Ce^{3+}{}_xO$ (x= 0.00, 0.03, 0.07, 0.15) were prepared by the co-precipitation method [17] using an aqueous solution of $Mg(NO_3)_2.6H_2O$ (0.1M) and $Ce(NO_3)_3.6H_2O$ and 1M K_2CO_3 as precipitants. Precipitant filtering and soaking the sample in hot water was then carried out followed by drying the sample (120 °C for 12 h). Successively, the pre-calcination of the sample took place in an open furnace to discard the CO_2 from the precipitant for 5 h at 500 °C. The sample was then pressed into disks (600 kg/m^2), followed by 20 h of calcination at 1150 °C to increase the mechanical properties and ensure an efficient interaction between the promoter (Ce_2O_3) and the support (MgO).

Impregnation of Co (1%) was achieved using the dichloromethane-dissolved $Co(C_5H_7O_2)_2$ following which, the catalysts were dried at 120 °C for 12 h. The dried catalysts were then grinded and sieved into particles of (with a diameter of 80–150 or 150–250 μm). Similar steps were applied for the $Co(acac)_2$/ $Mg_{1-x}Ce^{3+}{}_xO$ (x = 0.03, 0.07, 0.15) catalysts.

2.3 Catalysts Characterization

X-ray diffractometer (Shimadzu model XRD-6000) was utilized in this study and the crystals size was calculated using the Debye-Scherrer relationship [18]. Kratos Axis Ultra DLD system fixed with a monochromatic Al Kα (1486.6 eV) and Al and Mg X-ray sources were used to acquire the X-ray photoelectron spectroscopy (XPS) results. The operation of the X-ray gun (source of excitation) was carried out on an emission current of 20 mA combined with 15 kV voltages (Kratos Analytical Limited) [19]. Pass energy size was fixed at 100 and 40 eV. Region of interest for both the photo electron signals (O1s, Mg2p, Co2p and Ce3d) and the narrow scan were similar to each other. A Philips glass diffraction X-ray tube of broad focus at 2.7 kW was used for the radiation process.

The H_2-temperature programmed reduction (TPR) analysis (Thermo Fisher - Thermo Finnegan TPDRO 1100, accompanied by a thermal conductivity detector) for the calcined samples was carried out at a 10 °C/min heating rate and a 50–1000 °C temperature range. For the provision of the reducing atmosphere, 5% H_2/Ar flow was fed during the analysis. Additional TPR experiments were carried out using similar conditions at a temperature range of 50–700 °C to measure the degree of reduction of each catalyst. The degree of reduction was calculated utilizing the following equation from the integration of the peak area under the TPR profile at 700 °C and 1000 °C, respectively.

The total catalyst's surface area was measured using the Brunauer-Emmett-Teller (BET) method with nitrogen adsorption set at –196 °C. For the analysis, Thermo Fisher Scientific S.P.A (model: Surfer Analyzer, Thermo Fisher Scientific) nitrogen adsorption-desorption analyzer was adopted. An apparatus for transmission electron microscopy (TEM), Hitachi H7100 TEM with an increasing voltage (10 MV) was used to diagnose the crystal system and the catalyst's homogeneity. Mettler Toledo TG-DTA (Pt crucibles, Pt/Pt-Rh thermo-couple) with a heating range of 50 to 1000 °C was used to carry out the thermo-gravimetric analysis (TGA).

2.4 Catalytic Evaluations

Syngas production (H_2/CO) for the reforming of biogas was achieved using a fixed bed stainless steel micro-reactor (i.d. Ø = 6 mm, h = 34 cm). A mass flow gas controller (SIERRA instruments) and an online gas chromatography (GC) (Agilent 6890N; G 1540N) equipped with

Copyright © 2021, ISSN 1978-2993

Varian capillary columns HPPLOT/Q and HP-MOLSIV were connected to a reactor. Prior to the initiation of the process, a lowering of the catalyst to about 0.02 g was conducted by flowing 5% H_2/Ar at 700 °C, and holding for 3 h. The purpose of the reduction step was to convert the (Ni^{2+}, Pd^{2+}, and Pt^{2+}) phase of the catalyst to the metal (Ni, Pd, and Pt) phase at the active sites of the catalysts. The temperature of the reaction was maintained and checked using the thermo-couple placed into the catalyst chamber. The calculations of the CH_4 and CO_2 conversions and the selectivity of H_2 and CO, as well as syngas (H_2/CO) ratios were based on Eqs. (6)–(10):

$$CH_4\ Conversion\,\% = \frac{(CH_4)_{in} - (CH_4)_{out}}{(CH_4)_{in}} \times 100 \quad (6)$$

$$CO_2\ Conversion\,\% = \frac{(CO_2)_{in} - (CO_2)_{out}}{(CO_2)_{in}} \times 100 \quad (7)$$

$$H_2\ Selectivity\,\% = \frac{(H_2)}{2\left[(CH_4)_{in} - (CH_4)_{out}\right]} \times 100 \quad (8)$$

$$CO\ Selectivity\,\% = \frac{(CO)}{2\left[(CH_4)_{in} - (CH_4)_{out}\right] + \left[(CO_2)_{in} - (CO_2)_{out}\right]} \times 100 \quad (9)$$

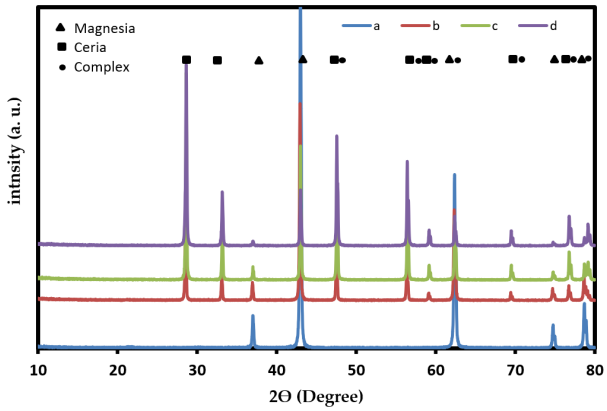

Figure 1. XRD patterns of the (a) Co/MgO (b) Co/$Mg_{0.97}Ce^{3+}_{0.03}O$ (c) Co/$Mg_{0.93}Ce^{3+}_{0.07}O$ and (d) Co/$Mg_{0.85}Ce^{3+}_{0.15}O$ catalysts.

$$H_2/CO\ ratio = \frac{H_2\ Selectivity\,\%}{CO\ Selectivity\,\%} \quad (10)$$

3. Results and Discussions

3.1 Catalysts Characterization

3.1.1 Patterns of XRD

The catalysts patterns of XRD are demonstrated in Figure 1. MgO reflections were observed by the wide-angle XRD patterns of Ce_2O_3-MgO catalyst supported by cobalt . The peaks of diffraction due to the cubic form of magnesia (JCPDS File No.: 00-002-1207) were recorded at approximately 2θ= 79.1° (222), 74.7° (311), 62.3° (220), 42.9° (200), and 37.0° (111) [19]. On the other hand, the peaks of diffraction at approximately 2θ= 79.1° (420), 76.7° (331), 69.4° (400), 59.1° (222), 56.4° (311), 47.5° (220), 33.1° (200), and 28.6° (111), were due to the form of ceria (cubic) (JCPDS File No.: 00-034-0394). The peaks due to the catalyst complex (Co-Ce-Mg-O) cubic form were observed at 2θ= 79.3° (318), 77.0° (317), 69.7° (224), 62.5° (104), 59.3° (304), 56.5° (115), and 47.7° (116). However, no diffraction peaks were observed for the 1% Co catalyst in all the patterns because of the minimal amount of these elements. A cubic form was recorded for the crystal system of all samples due to the cubic shaped particles in the catalyst [20]. XRD findings were supported by FE-SEM and TEM results.

The method of XRF was utilized for all the catalyst's components elemental analysis. Table 1 displays the cobalt percentage (slightly > 1) due to the incomplete precipitation of the metal precursors, Ce and Mg in the method of co-precipitation affecting the results to a minor extent [18].

3.1.2 XPS analysis

The analysis of XPS was implemented to study the reduced catalyst's (Co/$Mg_{0.85}Ce^{3+}_{0.15}O$) surface composition. An XPS examination of the surface of the catalysts

Table 1. Particle size measurement by XRD, TEM and XRF results.

Catalysts	TEM (nm)	Crystal size (D) Debye-Sherrer's eq. (nm)[a]	XRF	
			Co%	Mg & Ce%
Co/MgO	46	49.4	0.89	97.34
Co/$Mg_{0.97}Ce^{3+}_{0.03}O$	52	52.6	0.92	96.89
Co/$Mg_{0.93}Ce^{3+}_{0.07}O$	55	53.1	1.05	97.46
Co/$Mg_{0.85}Ce^{3+}_{0.15}O$	58	61.4	1.10	97.11

[a] Determined by the Debye-Scherrer's equation of the Mg (200) plane of XRD

Copyright © 2021, ISSN 1978-2993

with 3-12 nm displayed the photoelectron signals emittance from Co2p, Mg2p, Ce3d, and O1s as shown in Figure 2(a-d). The photoelectron signal, O1s, displayed the peaks for Mg–O, Ce–O, and Co–O, that were deconvoluted at binding energies 530, 529.2, and 529.1 eV, respectively, as shown in Figure 2b. The narrow scan of the XPS spectra for the Mg2p region of the nano-catalyst recorded one peak at 47 eV (binding energy) (Figure 2c). Whereas, the other peaks located at the binding energies around 787 and 795 eV were assigned to the Co2p. Finally, the narrow scan of XPS spectra for the Ce3d region of the nano-catalyst deconvoluted into complex peaks and demonstrated the strongest photoelectron signal intensity at binding energies of 917, 905, 900, 896, 887 and 880 eV, in comparison with the other peaks. The Ce3d, Mg2p [18], and Co2p narrow scan displayed a combination of Ce–O, Mg–O, and Co–O in the metal's composition of the oxide species respectively [21].

3.1.3 Surface Area of Brunauer-Emmett-Teller (BET)

The surface area values of BET (S_{BET}) along with the reduced catalyst supports pore properties are displayed in Table 2. A 17.6 Å pore radius, 0.064 cm^3/g pore volume, and a 9.5 m^2/g surface area were recorded for the Co/MgO catalyst. Nonetheless, an increase in the surface area and volume was noticed upon the addition of Ce_2O_3 (promoter). This elevation may be attributed to the strong interaction between the metal (Co) and support (MgO–Ce_2O_3). The current findings are concurrent with the findings by earlier reports [22]. However, by adding Ce_2O_3 at a temperature of 1150 °C, the loss of the surface area during calcination has been curbed, resulting in an increase in the catalyst surface area (Table 2). The surface areas for $Co/Mg_{0.97}Ce^{3+}_{0.03}O$, $Co/Mg_{0.93}Ce^{3+}_{0.07}O$ and $Co/Mg_{0.85}Ce^{3+}_{0.15}O$ catalysts were 13.4, 17.4, and 19.2 m^2/g, respectively.

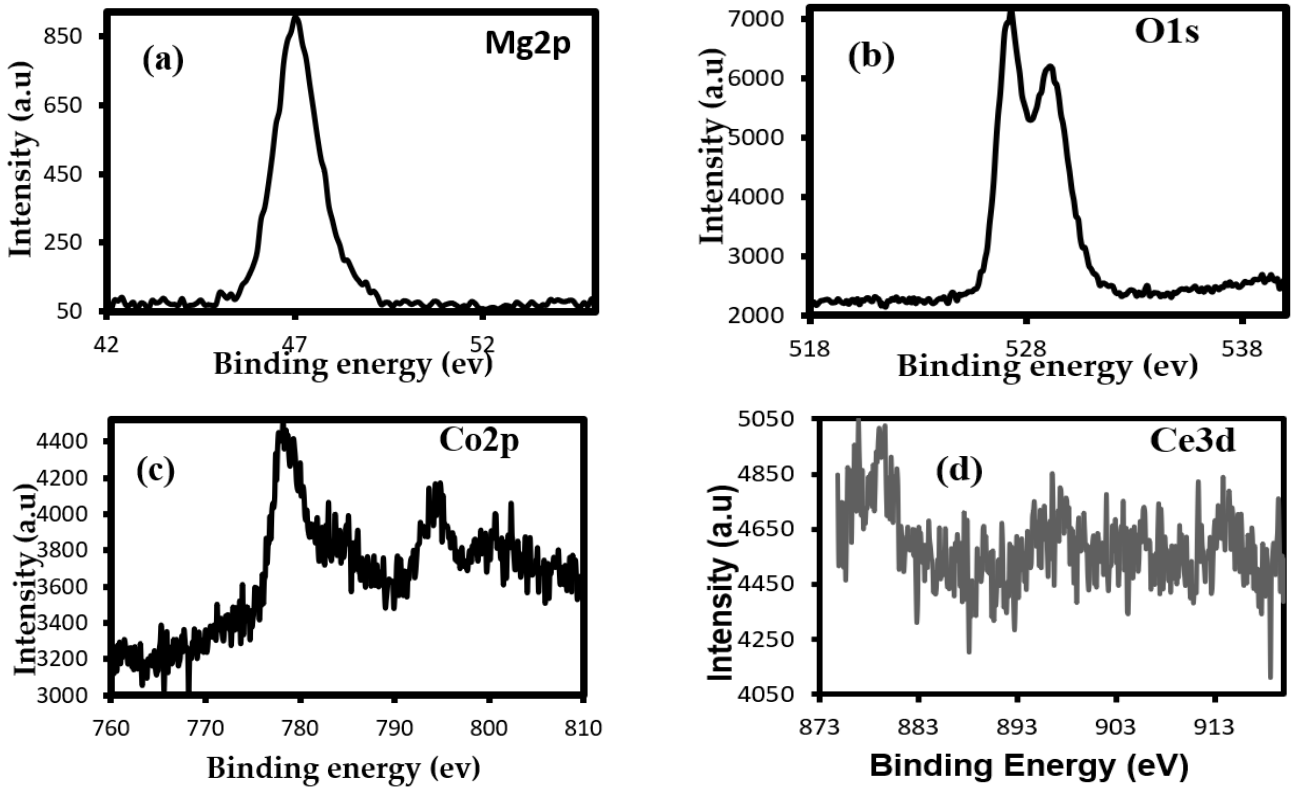

Figure 2. Narrow XPS of the $Co/Mg_{1-x}Ce_xO$ catalyst. (a) Mg2p (b) O1s; (c) Co2p (d) Ce3d.

Table 2. The main textural properties of fresh catalysts from BET method.

Sample name	Specific surface area (m^2/g)	Pore volume (cm^3/g)	Pore radius (Å)
Co/MgO	9.5	0.064	17.6
$Co/Mg_{0.97}Ce^{4+}_{0.03}O$	13.4	0.105	24.3
$Co/Mg_{0.93}Ce^{4+}_{0.07}O$	17.4	0.145	38.8
$Co/Mg_{0.85}Ce^{4+}_{0.15}O$	19.2	0.153	52.7

Copyright © 2021, ISSN 1978-2993

An increase in the surface area was observed upon the increase in the amount of Ce. The pore radius of all the catalysts was affected by the Ce_2O_3 concentration level. A pore radius of 24.3, 38.8 and 52.7 Å was recorded for the catalysts Co/$Mg_{0.97}Ce^{3+}_{0.03}O$, Co/$Mg_{0.93}Ce^{3+}_{0.07}O$ and Co/$Mg_{0.85}Ce^{3+}_{0.015}O$, respectively. The pore volume slightly increased following the addition of cerium to 0.105, 0.145 and 0.153 cm^3/g for Co/$Mg_{0.97}Ce^{3+}_{0.03}O$, Co/$Mg_{0.93}Ce^{3+}_{0.07}O$ and Co/$Mg_{0.85}Ce^{3+}_{0.015}O$ catalysts, respectively.

3.1.4 TEM characterization

Figure 3(a-d) demonstrates the TEM images of the synthesized catalysts distribution and morphology. The particle size and cubic structures were analysed by TEM to characterize crystals at approximately 40–80 nm (smallest). Regular shaped particles were observed by the catalysts Co/MgO, Co/$Mg_{0.97}Ce^{3+}_{0.03}O$, Co/$Mg_{0.93}Ce^{3+}_{0.07}O$, Co/$Mg_{0.85}Ce^{3+}_{0.15}O$. Meanwhile, the cobalt metal uniformly supported the regular shape of the support and together formed a smaller particle size and resulted in a considerable homogeneity in metal dispersion. Figure 3(a-d) shows a 2D cubic texture devoted to the catalyst [23]. The pores of the catalyst were of uniform size (~18 nm) which concurred with the findings from the BET as sown in Table 2. Several particles of cobalt were loaded on the external surface of the support

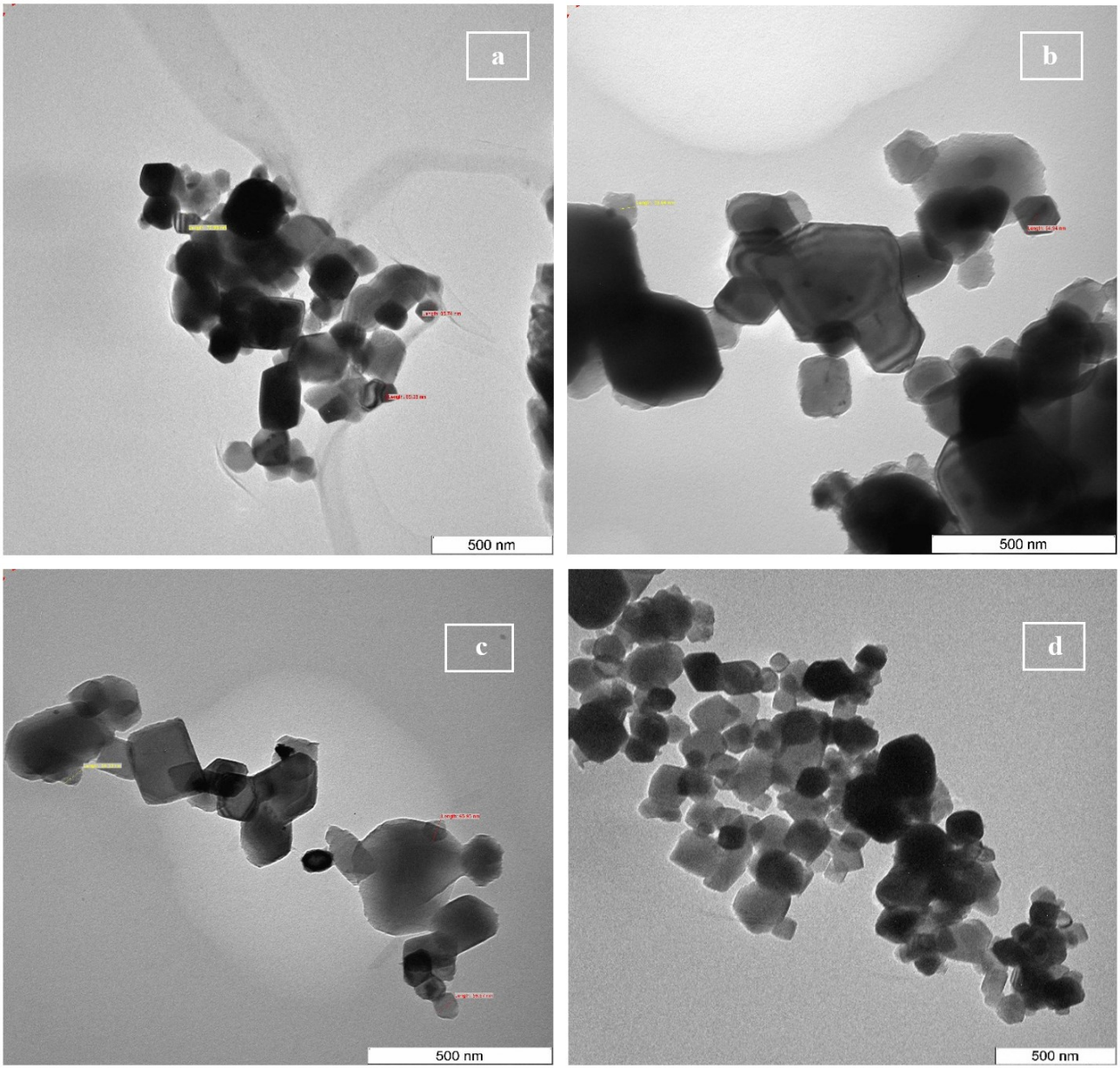

Figure 3. TEM image of catalysts (a) Co/MgO (b) Co/$Mg_{0.97}Ce^{3+}_{0.03}O$ (c) Co/$Mg_{0.93}Ce^{3+}_{0.07}O$ (d) Co/$Mg_{0.85}Ce^{3+}_{0.15}O$.

Copyright © 2021, ISSN 1978-2993

$Mg_{0.85}Ce^{3+}_{0.15}O$ uniformly, which differed from the crystalline sites within the porous structure. The reduced homogeneity of Co particle as compared to other catalysts (due to the regulated crystal growth in the narrowly distributed channels) can explain the discrepancy in the metal particle sizes. The increase in the supported cobalt particle size was in the following sequence; Co/MgO < $Co/Mg_{0.97}Ce^{3+}_{0.03}O$ < $Co/Mg_{0.93}Ce^{3+}_{0.07}O$ < $Co/Mg_{0.85}Ce^{3+}_{0.15}O$, corresponding to the Scherrer equation results (Table 1).

3.1.5 Temperature programmed reduction (H_2-TPR)

The reducibility of cerium for the reforming of cobalt catalysts was characterized by H_2-TPR. Table 3 demonstrates the profiles of H_2-TPR for $Co/Mg_{1-x}Ce^{3+}_xO$ (where x= 0.00, 0.03, 0.07, 0.15) and Figure 4(a-d) illustrates the catalysts patterns. A reduction in the crystallite Co-O may have caused the occurrence of the Co/MgO catalyst peak at the temperature of 540 °C [24]. Figure 4(b-d) demonstrates the H_2-TPR profiles for $Co/Mg_{0.97}Ce^{3+}_{0.03}O$, $Co/Mg_{0.93}Ce^{3+}_{0.07}O$, and $Co/Mg_{0.85}Ce^{3+}_{0.15}O$. The first peak was formed for $Co/Mg_{0.97}Ce^{3+}_{0.03}O$, $Co/Mg_{0.93}Ce^{4+}_{0.07}O$, and $Co/Mg_{0.85}Ce^{3+}_{0.15}O$ at temperatures of 560 °C, 553 °C, and 544 °C respectively, due to the reduction of Co-O to Co^0. The second peak for $Co/Mg_{0.97}Ce^{3+}_{0.03}O$, $Co/Mg_{0.93}Ce^{3+}_{0.07}O$, and $Co/Mg_{0.85}Ce^{3+}_{0.15}O$ at temperatures of 464 °C, 470 °C, and 473 °C respectively, corresponded to the Ce_2O_3 reduction on the surface of the $Co/Mg_{1-x}Ce^{3+}_xO$ catalysts. Meanwhile, the third peak was formed at temperatures 710 °C, 735 °C, and 797 °C for $Co/Mg_{0.97}Ce^{3+}_{0.03}O$, $Co/Mg_{0.93}Ce^{3+}_{0.07}O$, and $Co/Mg_{0.85}Ce^{3+}_{0.15}O$, respectively, and was attributed to the reduction of Ce_2O_3 in the bulk of the catalysts. The reduction in the second peak's temperature as compared to the third peak was attributed to the reduction enthalpies. This may be due to the incorporation of MgO into Ce_2O_3 and the hindrance of sintering that enhances the dispersion of Ce_2O_3 particles [22,25]. The other possible explanation may be due to the stronger interaction between Ce_2O_3 and cobalt metal [26]. The H_2-consumption of 281.1 µmol/g catalyst was used for the reduction of total Co-O to Co on Co/MgO. The total H_2-consumption's amount of the reduced catalysts $Co/Mg_{0.97}Ce^{3+}_{0.03}O$, $Co/Mg_{0.93}Ce^{3+}_{0.07}O$, and $Co/Mg_{0.85}Ce^{3+}_{0.15}O$ was recorded at 360.6, 417.4 and 611.5 µmol/g respectively, as calculated from the three peak areas indicating a possible Co–O reduction, and a partial Ce_2O_3 reduction. An enhancement in the reducibility of the catalysts was observed following the addition of the Ce_2O_3 promoter, especially the catalysts with MgO support possibly as a result of the support's acidic-basic properties. As the Ce_2O_3 content in the catalyst increased, it became easier to reduce the catalyst using H_2, indicating a higher presence of the active sites, hence, an increase in the conversion rate of CH_4 and CO_2 in the catalyst $Co/Mg_{0.85}Ce^{3+}_{0.15}O$. It is clear that $Mg_{1-x}Ce^{3+}_xO$ (higher basicity as compared to

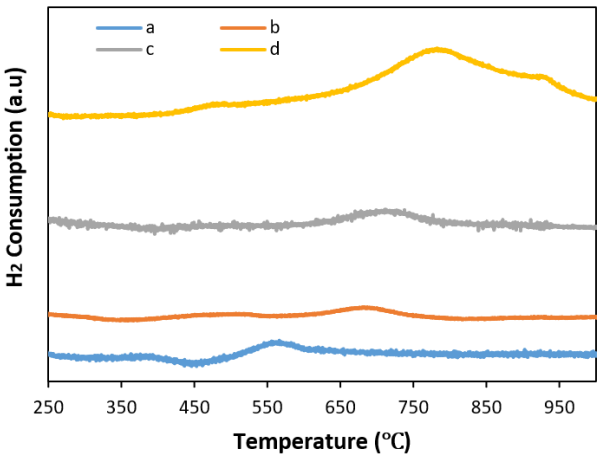

Figure 4. H_2-TPR profiles of (a) Co/MgO (b) $Co/Mg_{0.97}Ce_{0.03}O$ (c) $Co/Mg_{0.93}Ce_{0.07}O$ (d) $Co/Mg_{0.85}Ce_{0.15}O$ catalysts, (reduced in a 5% H_2/Ar stream at a 10 °C/min temperature ramp).

Table 3. H_2-TPR values of the different catalysts.

Catalysts	Temperature (°C)			Amount H_2-gas adsorbed (µmol/g)	Reduction degree (%)[a]
Co/MgO	540	-----	-----	281.1	70
$Co/Mg_{0.97}Ce^{3+}_{0.03}O$	560	464	710	360.6	89
$Co/Mg_{0.93}Ce^{3+}_{0.07}O$	553	470	735	417.4	92
$Co/Mg_{0.85}Ce^{3+}_{0.15}O$	544	473	797	611.5	100

[a] Reduction degree (%)= (H_2 consumption amount 700 °C / H_2 consumption amount 1000 °C) x 100.

Copyright © 2021, ISSN 1978-2993

MgO) strongly interacted with Ce_2O_3 promoter and resulted in a better Co-O reduction concerning the redox property of $Mg_{1-x}Ce^{3+}{}_xO$ [18].

3.1.6 Thermal analysis

The catalysts Co/MgO, $Co/Mg_{0.97}Ce^{3+}{}_{0.03}O$, $Co/Mg_{0.93}Ce^{3+}{}_{0.07}O$, and $Co/Mg_{0.85}Ce^{3+}{}_{0.15}O$ components are illustrated by Figure 5(a-d). At first, due to the N_2 gas adsorption on the compound, a slight weight increase was noted. A weight loss of 4% and 2%, was recorded for the Co/MgO and $Co/Mg_{0.93}Ce^{3+}{}_{0.07}O$, respectively, which may be due to the moisture removal from the $Co/Mg_{1-x}Ce^{3+}{}_xO$ catalysts, whereas, the results for the $Co/Mg_{0.97}Ce^{3+}{}_{0.03}O$ and $Co/Mg_{0.85}Ce^{3+}{}_{0.15}O$ catalysts were stable despite the increase in temperature, indicating the thermal stability of the compounds. Thermal stability for the compounds was achieved at 500 °C, corresponding to the elevated melting point of Ceria (2177 °C) and Magnesia (2852 °C) that resulted in a good interaction among the components of the catalyst. The thermal analysis findings were consistent with the results by Gaddalla [27].

3.2 The Performance of Catalyst in Biogas Reforming

3.2.1 The role of the concentration of the reactant on conversion

The CH_4 and CO_2 conversion, and the selectivity (H_2/CO ratio) revealed the activity of the dry reforming reaction. Upon an increase in the temperature to 900 °C, CO and H_2 were observed in the outlet gas of the blank tests (reaction without catalyst) which may be attributed to the reaction of decomposition of methane (Eq. (3)). Using $Mg_{1-x}Ce^{3+}{}_xO$ without the main catalyst (metals) resulted in lowering the CH_4 conversion (32%) and CO_2 (41%) with an H_2/CO ratio of 0.3% indicating the possibility of a weak reaction on the promoter-support pores as presented by the results of the BET. On the contrary, when using the catalyst $Co/Mg_{1-x}Ce^{3+}{}_xO$, an elevation in the rate of CH_4 and CO_2 conversion and the H_2/CO ratio was observed. Figure 6 demonstrates the effects of the reactant (CH_4:CO_2) ratio on the CH_4, CO_2 conversion, and H_2/CO ratio. The reaction was conducted using two ratios of (CH_4:CO_2); 1:1 and 2:1. By increasing the CO_2 concentration in the (CH_4:CO_2) ratio to 1:1, the CH_4 and CO_2 conversion and the H_2/CO ratio were increased due to the decline in the carbon deposition on the catalyst that produced CO by reacting with the excess CO_2 (Eq. 5). Besides, the role of the doped cobalt metal on the promoter-support in the catalytic reaction was imperative. It has been noted that the most CH_4 (75%) and CO_2 (86 %) conversion was observed by $Co/Mg_{0.85}Ce^{3+}{}_{0.15}O$ catalyst with a 1:1 of CO_2 : CH_4, and a 1.0 H_2/CO ratio. Nevertheless, at a 2:1 ratio, the conversion of the CO_2 and CH_4 gases was recorded at 77% and 68%, respectively with a 0.8 H_2/CO ratio. This finding demonstrated that the best deactivate resistance of the catalyst stands at a 1:1 ratio due to the decline in carbon formation which leads to a high H_2 and CO selectivity (Figure 6). Similar findings were also acquired by the other catalysts reported previously [28].

3.2.2 The role of the concentration of the catalyst on conversion

The role of the catalyst concentrations on the conversion process is illustrated by Figure

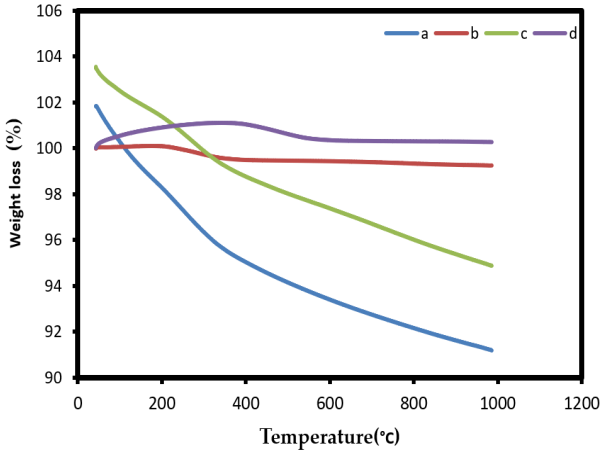

Figure 5. TGA of the catalysts (a) Co/MgO (b) $Co/Mg_{0.93}Ce^{3+}{}_{0.07}O$ (c) $Co/Mg_{0.97}Ce^{3+}{}_{0.03}O$ (d) $Co/Mg_{0.85}Ce^{3+}{}_{0.15}O$.

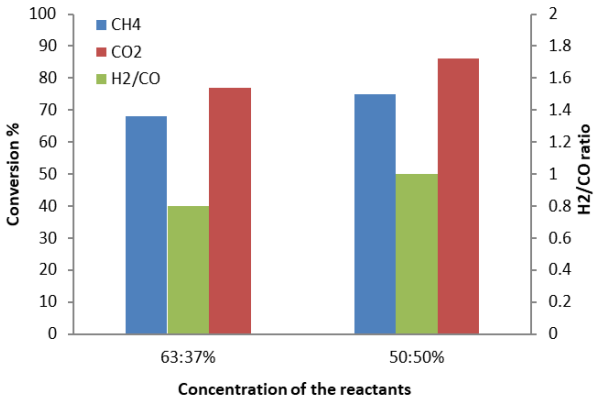

Figure 6. The effect of changing the ratio concentration of CH_4:CO_2 reactant 1- 2:1 2- 1:1 over the percentage of their conversion and H_2/CO ratio for $Co/Mg_{0.85}Ce^{3+}{}_{0.15}O$ catalyst at 900 °C

Copyright © 2021, ISSN 1978-2993

7 and Table 4. The CH_4 and CO_2 conversion values and H_2/CO ratio for the catalyst Co/MgO were 48%, 62% and 0.6, whereas for the $Co/Mg_{0.97}Ce^{3+}{}_{0.03}O$ catalyst, the values were 68%, 74% and 0.7 and for the $Co/Mg_{0.93}Ce^{3+}{}_{0.07}O$ catalyst, the values were 72%, 79% and 0.8. The highest values for the CH_4 and CO_2 conversion and H_2/CO ratio for the $Co/Mg_{0.85}Ce^{3+}{}_{0.15}O$ catalyst was reported to be 75%, 86%, and 1.0, respectively.

The initial conversion trend of CH_4 and CO_2 concurred with the number of Co^0 active sites, indicating the significance of the degree of reduction in the Co/Mg−Ce−O based catalyst system. On the contrary, the catalysts pre-reduction was achieved at 700 °C, due to the DRM operating temperature in the current study (700 °C). As can be seen in the TPR results, the 700 °C reduction temperature was inadequate for the reduction of the complex CoO species in the $Co/Mg_{1-x}Ce_xO$ catalysts. The degree of reduction calculations can be implemented to get a quantitative analysis of the catalyst's reducibility [29]. The estimated degree of reduction values are displayed in Table 3. An estimated value of 100% was obtained for

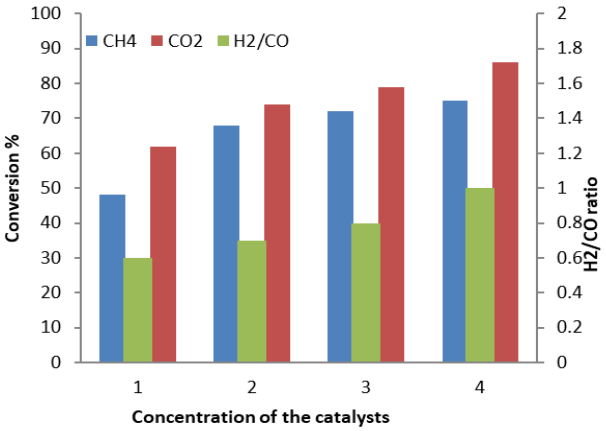

Figure 7. The effect of using different catalysts (1) Co/MgO, (2) $Co/Mg_{0.97}Ce^{3+}{}_{0.03}O$ (3) $Co/Mg_{0.93}Ce^{3+}{}_{0.07}O$, and (4) $Co/Mg_{0.85}Ce^{3+}{}_{0.15}O$ on CH_4, CO_2 conversion and H_2/CO ratio at 900 °C for the 1:1 ratio of CH_4:CO_2

the $Co/Mg_{0.85}Ce_{0.15}O$ catalyst owing to its easier reducibility. Hence, the high $Co/Mg_{0.85}Ce_{0.15}O$ catalytic activity can be attributed to the complete complex CoO species conversion into Co^0. The degrees of reduction exhibited by the $Co/Mg_{0.93}Ce_{0.07}O$, $Co/Mg_{0.97}Ce_{0.03}O$, and Co/MgO catalysts were 92, 89, and 70%, respectively, whereas a fraction of the complex CoO species stayed in the inactive oxide form.

Positive findings in the present study may have been due to the favorable cobalt metal interaction with the promoter-support and the good Ce_2O_3-MgO catalyst basicity. Unfavorable results were previously reported by Laosiripojana [30] and Guo *et al.* [31] due to the usage of the catalyst Ni/Al_2O_3 which demonstrated a weak interaction between the support and Ni and low Al_2O_3 basicity.

H_2/CO ratio and CO_2 and CH_4 conversion for the catalysts decreased in the following order $Co/Mg_{0.85}Ce^{3+}{}_{0.15}O$ > $Co/Mg_{0.93}Ce^{3+}{}_{0.07}O$ > $Co/Mg_{0.97}Ce^{3+}{}_{0.03}O$ > Co/MgO indicating that the most efficient catalyst among the other studied catalysts was $Co/Mg_{0.85}Ce^{3+}{}_{0.15}O$. Findings clarified the dependency of the rate of formation of the H_2 and CO gases in the DRM reaction on the amount of solid solution, MgO-Ce_2O_3 in the catalyst. As such, the more the amount of the solid solution MgO−Ce_2O_3, the more the H_2 and CO gases formation rate. Hence, the role of the solid solution MgO−Ce_2O_3 formation is crucial in the generation of active sites for the DRM reaction. This occurs due to the capacity of the entire Ce_2O_3 in stabilizing both oxides. In the catalyst, reduction at 700 °C was only observed at the surface of the Ce_2O_3 of the solid solution, MgO−Ce_2O_3. The generated Ce sites remained in close vicinity with the solid solution hindering Ce sintering [32]. Table 4 illustrates the $Co/Mg_{1-x}Ce^{3+}{}_xO$ selectivity and activity (higher than that of $Co/Mg_{1-x}Ce^{3+}{}_xO$) in the reaction of DRM.

Moreover, the elevation in the CH_4 and CO_2 conversion rate was due to the particle size involved in the activity of the reaction. Using the TEM analysis and the equation of Debye Sher-

Table 4. The catalytic results of DRM reaction for the catalysts at 900 °C for the 1:1 ratio of CH_4:CO_2.

Sample name	CH_4 Conversion%	CO_2 Conversion %	H_2/CO ratio
MgO	21	32	0.1
$Mg_{0.85}Ce^{3+}{}_{0.15}O$	32	41	0.3
Co/MgO	48	62	0.6
$Co/Mg_{0.97}Ce^{3+}{}_{0.03}O$	68	74	0.7
$Co/Mg_{0.93}Ce^{3+}{}_{0.07}O$	72	79	0.8
$Co/Mg_{0.85}Ce^{3+}{}_{0.15}O$	75	86	1.0

Copyright © 2021, ISSN 1978-2993

rer's, the Co doping metal was prepared with a particle size as minuscule as nanoparticles. Hence, the crucial role of the particle size is evident in the activity of the reaction. Elevation in the reactant's selectivity (yield) and conversion may be a result of the decrease of the particles into nano-ranged sizes, along with having the highest BET surface area (19.2 m^2/g) (Table 2) and the highest H_2-consumption in H_2-TPR (611.5 µmol/g of active sites) (Table 3).

3.2.3 The role of temperature on the conversion

The $Co/Mg_{0.85}Ce^{3+}{}_{0.15}O$ catalyst selectivity and activity at a temperature range of 700–900 °C can be seen in Figure 8. Generally, an enhancement in the CH_4:CO_2 ratio of (1:1) was noted upon increasing the temperature from 700–900 °C which may be attributed to the strong endothermic nature of the dry reforming of methane reaction (Eq. (1)). Earlier research reported an increase in the rate of conversion at higher temperatures [33]. It is noted that an elevation in the temperature (700–900 °C) led to an increase in the CH_4 conversion of $Co/Mg_{0.85}Ce^{3+}{}_{0.15}O$ (42% to 75%) and an elevation in the CO_2 conversion from 53% to 86%. However, at a temperature higher than 900 °C, no evident elevation in the CO_2 and CH_4 conversion rates was observed. Figure 8 illustrates the catalyst H_2/CO ratio at a range of temperatures. At a temperature lower than 900 °C, the recorded sample's H_2/CO ratio was <1. The lowering in the ratio of H_2/CO may be due to the extra H_2 in the reverse water-gas-shift reaction (RWGS), to produce CO [Eq. (2)]. At a temperature of 900 °C, the $Co/Mg_{0.85}Ce^{3+}{}_{0.15}O$ catalyst's H_2/CO ratio was recorded at 1.0, indicating a small contribution from the RWGS reaction (Eq. (2)) [34].

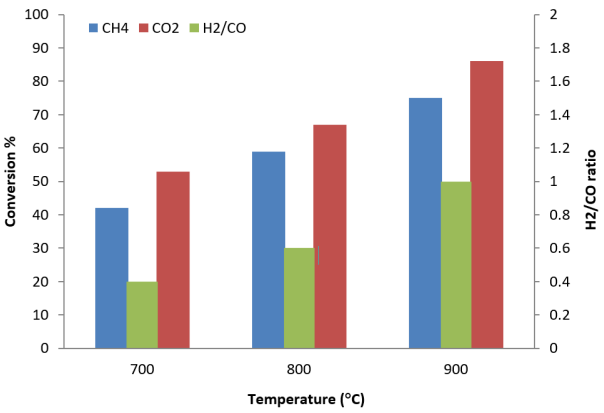

Figure 8. The influence of temperature on the catalytic activity of the $Co/Mg_{0.85}Ce^{3+}{}_{0.15}O$ catalyst. (1) 700 °C (2) 800 °C (3) 900 °C for the 1:1 ratio of CH_4:CO_2.

3.2.4 Stability tests

As can be seen in Figure 9, a high rate of methane and carbon dioxide diffusion was observed at a temperature of 900 °C. Initially, the adsorption of Methane on the nickel's catalyst surface took place to yield hydrogen resulting in the accumulation of carbon on the nickel's surface as can be seen below (Eqs. (11)–(15)) [17].

$$CH_4 + 2Co \rightarrow CH_3Co + HCo \quad (11)$$
$$CH_3Co + Co \rightarrow CH_2Co + HCo \quad (12)$$
$$CH_2Co + Co \rightarrow CHCo + HCo \quad (13)$$
$$CHCo + Co \rightarrow CCo + HCo \quad (14)$$
$$2HCo \rightarrow H_2 + 2Co \quad (15)$$

Secondly, Aldoghachi *et al.* [17] had demonstrated the role of the catalyst promoter (Ce_2O_3) on the dry reforming reaction in which CO_2 was activated on the Ce metal particle as (Eqs. (16)–(20)):

$$CO_{2\,g} \rightarrow CO_{2\,support} \quad (16)$$
$$CO_{2\,support} + O^{-2}{}_{support} \rightarrow CO_{3\,support}{}^{-2} \quad (17)$$
$$2H_{metal} \rightarrow 2H_{support} \quad (18)$$
$$CO_{3\,support}{}^{-2} + 2H_{support} \rightarrow HCO_{2\,support}{}^{-1} + OH^{-1}{}_{support} \quad (19)$$
$$CO_{support} \rightarrow CO_{g} \quad (20)$$

It has been known that the carbon deposition on the cobalt metal surface curbs the catalyst's stability, counteracted by the Ce_2O_3 promoter availability that reactivates the catalyst by eliminating the deposited carbon. The main reason behind the reaction lasting for ≥ 200 h was the utilization of the promoter Ce_2O_3 in the catalyst that helped ensure stability and a strong coke resistance. Ce_2O_3 also ensured the removal of the carbon formed on the catalyst during the reaction of DRM. This was followed by the carbonate types formation ($Ce_2O_2CO_3$), especially Ce_2O_3, that has the potential of

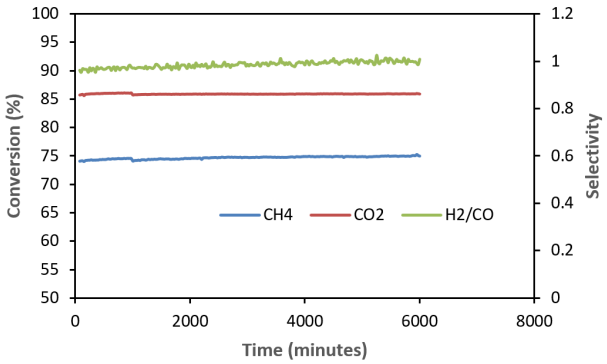

Figure 9. Stability tests of $Co/Mg_{0.85}Ce^{3+}{}_{0.15}O$ catalysts under 900 °C for the 1:1 ratio of CH_4:CO_2 for 200 h (GHSV = 15000 $mL \cdot gcat^{-1} \cdot h^{-1}$, atmospheric pressure).

Copyright © 2021, ISSN 1978-2993

changing carbon dioxide into O and CO. Lastly, an O atom was generated with the C that was deposited on the Co metal catalyst to yield CO. Based on the results, the deposition of carbon on the catalyst decreased significantly as can be seen below (Eqs. (21) and (22)):

$$CO_{2\,g} \rightarrow CO_{\,support} + O_{\,promoter} \quad (21)$$

$$C_{\,metal} + O_{\,promoter} \rightarrow CO_{\,g} \quad (22)$$

In conclusion, the above mechanism prevents the carbon deposition on the $Co/Mg_{0.85}Ce^{3+}{}_{0.15}O$ catalyst surface making the catalyst fit for long term usage.

3.2.5 Characterization of the catalyst post-reaction.

Evaluating the coke formation on the catalyst $Co/Mg_{0.85}Ce^{3+}{}_{0.15}O$ took place by the TPO-MS, TEM images, and BET post-reaction tests. There was no observed coke deposited on the catalyst surface as demonstrated by the TPO-MS profile (Figure 10). The spent $Co/Mg_{0.85}Ce^{3+}{}_{0.15}O$ catalyst's TEM analysis supported the above finding (Figure 11). Even following 200 h of stream testing, the original catalyst structure was maintained as can be seen in the figure. Moreover, the 2D-cubic texture of the spent catalyst was maintained. A slight elevation in the spent catalyst pore size from 52.7 Å to 57.9 Å was reported. The BET analysis also demonstrated a marginal increase from 19.2 to 20.1 m^2/g in the spent catalyst surface area. The absence of filamentous carbon on the spent catalyst concluded the negligibility of the deposition of coke.

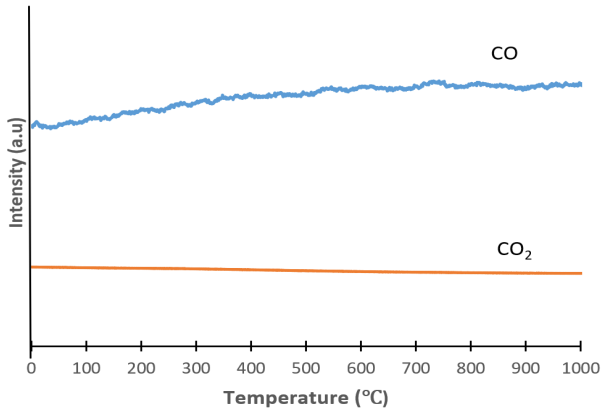

Figure 10. Temperature programmed oxidation TPO curves of spent $Co/Mg_{0.85}Ce^{3+}{}_{0.15}O$ catalyst after reaction at T = 900 °C for the 1:1 ratio of CH_4:CO_2 for 200 h (GHSV = 15000 $mL \cdot gcat^{-1} \cdot h^{-1}$, atmospheric pressure).

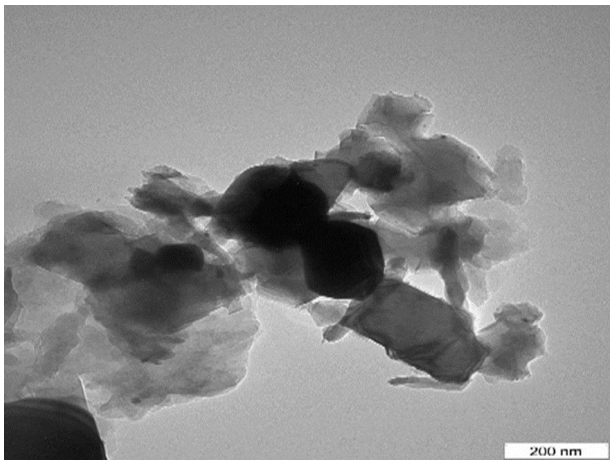

Figure 11. TEM analysis of spent $Co/Mg_{0.85}Ce^{3+}{}_{0.15}O$ catalyst after reaction: at 900 °C, and CH_4/CO_2 ratio of 1:1.

3.2.6 Improving the catalyst's activity and stability.

The DRM reaction can be improved by conducting research at a lower flow of oxygen (1.25%). As demonstrated by Figure 12, an enhancement in the CH_4 conversion (75% to 84%) following the addition of an oxidant (O_2, to partially or completely synthesize methane) and utilizing the exothermicity of the reaction (to provide the required heat directly to the DRM reactant mixture) was observed [17]. No effect was seen on the ratio of H_2/CO and the conversion of CO_2, may be due to the reaction of CH_4 with O to yield H_2O and CO (Eq. (23)). Lastly, syngas was produced as a result of the reaction of steam with the deposited carbon (Eq. (24)). O_2 has the potential of oxidizing the coke deposited on the catalyst (Eq. (25)), hence, reducing the deposition of carbon and improving the catalyst's lifetime.

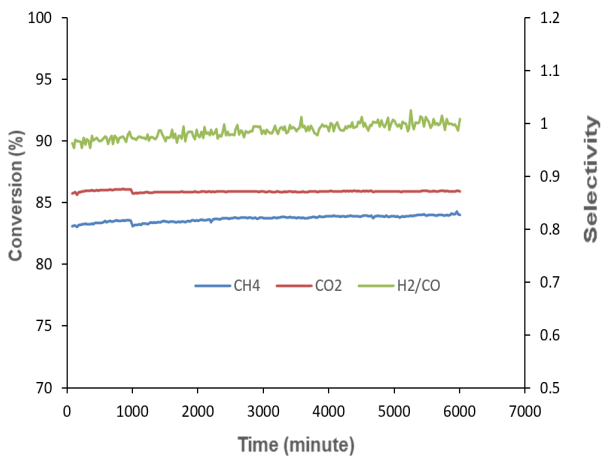

Figure 12. DRM reaction of the $Co/Mg_{0.85}Ce^{3+}{}_{0.15}O$ catalyst under 900 °C with 1.25% O_2.

Copyright © 2021, ISSN 1978-2993

$CH_4 + 3/2\ O_2 \rightarrow CO + 2H_2O$ (23)

$C + H_2O \rightarrow CO + H_2$ (24)

$C + 1/2\ O_2 \rightarrow CO$ (25)

4. Conclusion

The impact of several operating parameters on the reaction of DRM were studied in a fixed-bed reactor utilizing $Co/Mg_{1-x}Ce^{3+}{}_xO$ (x= 0, 0.03, 0.07, 0.15; 1 wt% cobalt each) catalysts prepared using the co-precipitation method with K_2CO_3 as precipitant. A high BET surface area (19.2 $m^2.g^{-1}$) was possessed by the $Co/Mg_{0.85}Ce^{3+}{}_{0.15}O$ catalyst along with an easier reducibility. TEM image showed a relatively uniform cubic shape with a diameter of about 58 nm. In addition, the formation of MgO phase on the surface of the catalyst with a dimension size of 61.4 nm was detected utilizing XRD patterns. Using H_2-TPR measurement, the reduction of CoO to metallic Co^0 phase was identified at different reduction temperatures dependent on the degree of metal-support interaction and the location of CoO particles on the surface or inside the channels of mesoporous $Mg_{0.85}Ce^{3+}{}_{0.15}O$ support. In general, the catalytic performance of the 1:1 ratio of CH_4:CO_2 for the $Co/Mg_{0.85}Ce^{3+}{}_{0.15}O$ catalyst for 200 h on-stream at 900 °C was unchanged with CH_4, CO_2 conversions and H_2/CO ratio of 75%, 86% and 1.0, respectively. TPO-MS and TEM images were implemented to evaluate the formation of coke on the catalyst $Co/Mg_{0.85}Ce^{3+}{}_{0.15}O$, post-reaction tests. No deposition of coke was observed on the catalyst surface and by conducting research at a lower flow of oxygen (1.25%), the conversion of CH_4 was improved from 75% to 84%.

Acknowledgements

This study was funded by the NanoMite Grant (Vot. No: 5526308). The authors would like to thank the chemistry department, Faculty of Science, UPM, for all the facilities provided.

References

[1] Istadi, I., Anggoro, D.D., Amin, N.A.S., Ling, D.H.W. (2011). Catalyst deactivation simulation through carbon deposition in carbon dioxide reforming over $Ni/CaO-Al_2O_3$ catalyst. *Bulletin of Chemical Reaction Engineering & Catalysis*, 6(2), 129–136, doi: 10.9767/bcrec.6.2.1213.129-136

[2] Omoregbe, O., Danh, H.T., Nguyen-Huy, C., Setiabudi, H.D., Abidin, S.Z., Truong, Q.D., Vo, D.V.N. (2017). Syngas production from methane dry reforming over Ni/SBA-15 catalyst: Effect of operating parameters. *International Journal of Hydrogen Energy*, 42(16), 11283–11294, doi: 10.1016/j.ijhydene.2017.03.146

[3] Al-Doghachi F.J. (2018) Effects of platinum and palladium metals on $Ni/Mg_{1-x}Zr_xO$ catalysts in the CO_2 reforming of methane. *Bulletin of Chemical Reaction Engineering & Catalysis*, 13(2), 295–310, doi: 10.9767/bcrec.13.2.1656.295-310

[4] Aboosadi, Z.A., Jahanmiri, A., Rahimpour, M.R. (2011). Optimization of tri-reformer reactor to produce synthesis gas for methanol production using differential evolution (DE) method. *Applied Energy*, 88(8), 2691–2701, doi: 10.1016/j.apenergy.2011.02.017

[5] Chen, W.H., Lin, B.J., Lee, M., Huang, H. (2012). One-step synthesis of dimethyl ether from the gas mixture containing CO_2 with high space velocity. *Applied Energy*, 98, 92–101, doi: 10.1016/j.apenergy.2012.02.082

[6] Sarkari, M., Fazlollahi, F., Ajamein, H., Atashi, H., Hecker, W.C., Baxter, L.L. (2014). Catalytic performance of an iron-based catalyst in Fischer-Tropsch synthesis. *Fuel Processing Technology*, 127, 163–170, doi: 10.1016/j.fuproc.2014.05.003

[7] Zhang, J., Wang, H., Dalai, A.K. (2007). Development of stable bimetallic catalysts for carbon dioxide reforming of methane. *Journal of Catalysis*, 249(2), 300–310, doi: 10.1016/j.jcat.2007.05.004

[8] Al-Doghachi, F.A., Taufiq-Yap, Y.H. (2017). Syngas production from the CO_2 reforming of methane over $Co/Mg_{1-x}Ni_xO$ catalysts. *Journal of Chemical Sciences*, 129(11), 1781–1786, doi: 10.1007/s12039-017-1396-x

[9] Ashok, J., Kawi, S. (2013). Steam reforming of toluene as a biomass tar model compound over CeO_2 promoted $Ni/CaO-Al_2O_3$ catalytic systems. *International Journal of Hydrogen Energy*, 38(32), 13938–13949, doi: 10.1016/j.ijhydene.2013.08.029

[10] Liu, Y., He, Z., Zhou, L., Hou, Z., Eli, W. (2013). Simultaneous oxidative conversion and CO_2 reforming of methane to syngas over Ni/vermiculite catalysts. *Catalysis Communications*, 42, 40–44, doi: 10.1016/j.catcom.2013.07.034

[11] Chen, Q.J., Zhang, J., Jin, Q.W., Pan, B.R., Kong, W.B., Zhao, T.J., Sun, Y.H. (2013). Effect of reflux digestion treatment on the catalytic performance of $Ni-CaO-ZrO_2$ nanocomposite catalysts for CO_2 reforming of CH_4. *Catalysis Today*, 215, 251–259, doi: 10.1016/j.cattod.2013.06.011

Copyright © 2021, ISSN 1978-2993

[12] Alabi, W.O., Sulaiman, K.O., Wang, H. (2020). Sensitivity of the properties and performance of Co catalyst to the nature of support for CO_2 reforming of CH_4. *Chemical Engineering Journal*, 390, 124486, doi: 10.1016/j.cej.2020.124486

[13] Paksoy, A.I., Caglayan, B.S., Aksoylu, A.E. (2015), A study on characterization and methane dry reforming performance of Co-Ce/ZrO_2 catalyst. *Appl. Catal. B Environ.*, 168, 164–174, doi: 10.1016/j.apcatb.2014.12.038

[14] Casanovas, A., Roig, M., Leitenburg, C.D., Trovarelli, A., Llorca, J. (2010), Ethanol steam reforming and water gas shift over Co/ZnO catalytic honeycombs doped with Fe, Ni, Cu, Cr, and Na. *Int. J. Hydrogen Energy*, 35, 7690–7698, doi: 10.1016/j.ijhydene.2010.05.099

[15] Jang, W.J., Jeong, D.W., Shim, J.O., Kim, H.M., Han, W.B., Bae, J.W., Roh, H.S. (2014), Metal oxide (MgO, CaO, and La_2O_3) promoted Ni-$Ce_{0.8}Zr_{0.2}O_2$ catalysts for H_2 and CO production from two major greenhouse gases. *Renew Energy*, 79, 91–95, doi: 10.1016/j.renene.2014.08.032

[16] Cavallaro, S., Mondello, N., Freni, S. (2001), Hydrogen produced from ethanol for internal reforming molten carbonate fuel cell. *J. Power Sources*, 102, 198–204, doi: 10.1016/S0378-7753(01)00800-X

[17] Al-Doghachi, F.A., Islam, A., Zainal, Z., Saiman, M.I., Embong, Z., Taufiq-Yap, Y.H. (2016), High Coke-Resistance Pt/$Mg_{1-x}Ni_xO$ Catalyst for Dry Reforming of Methane. *PloS One*, 11(1), 5862–5884, doi: 10.1371/journal.pone.0145862

[18] Al-Doghachi, F.A., Rashid U., Taufiq-Yap, Y.H. (2016). Investigation of Ce (III) promoter effects on the tri-metallic Pt, Pd, Ni/MgO catalyst in dry- reforming of methane. *RSC Advances,* 6(13), 10372–10384, doi: 10.1039/C5RA25869C

[19] Al-Najar, A., Al-Doghachi, F.A., Al-Riyahee, A.A., Taufiq-Yap, Y.H. (2020). Effect of La_2O_3 as a Promoter on the Pt,Pd,Ni/MgO Catalyst in Dry Reforming of Methane Reaction. *Catalysts*, 10(7), 750, doi: 10.3390/catal10070750

[20] Saha, B., Khan, A., Ibrahim, H., Idem, R. (2014). Evaluating the performance of non-precious metal based catalysts for sulfur-tolerance during the dry reforming of biogas. *Fuel*, 120, 202–217, doi: 10.1016/j.fuel.2013.12.016

[21] Hidalgo-Carrillo, J., Sebti, J., Marinas, A., Marinas, M., Sebti, S. & Urbano, F.J. (2012). XPS evidence for structure–performance relationship in selective hydrogenation of crotonaldehyde to crotyl alcohol on platinum systems supported on natural phosphates. *Journal of Colloid and Interface Science*, 382(1), 67–73, doi: 10.1016/j.jcis.2012.05.050

[22] Al-Doghachi, F.A., Rashid, U., Zainal, Z., Saiman, M.I., Taufiq Yap, Y.H. (2015). Influence of Ce_2O_3 and CeO_2 promoters on Pd/MgO catalysts in the dry-reforming of methane. *RSC Advances,* 5(99), 81739–81752, doi: 10.1039/C5RA15825G

[23] Tada, S., Shimizu, T., Kameyama, H., Haneda, T., Kikuchi, R. (2012). Ni/CeO_2 catalysts with high CO_2 methanation activity and high CH_4 selectivity at low temperatures. *International Journal of Hydrogen Energy*, 37(7), 5527–5531, doi: 10.1016/j.ijhydene.2011.12.122

[24] Li, G., Hu, L., Hill, J.M. (2006). Comparison of reducibility and stability of alumina-supported Ni catalysts prepared by impregnation and co-precipitation. *Applied Catalysis A: General*, 301(1), 16–24, doi: 10.1016/j.apcata.2005.11.013

[25] Al-Doghachi, F.A., Taufiq-Yap, Y.H. (2018). CO_2 reforming of methane over Ni/MgO catalysts promoted with Zr and La oxides. *ChemistrySelect*, 3(2), 816–827, doi: 10.1002/slct.201701883

[26] Mahoney, E.G., Pusel, J.M., Stagg-Williams, S.M., Faraji, S. (2014). The effects of Pt addition to supported Ni catalysts on dry (CO_2) reforming of methane to syngas. *Journal of CO_2 Utilization*, 6, 40–44, doi: 10.1016/j.jcou.2014.01.003

[27] Gaddalla, A.M., Sommer, M.E. (1989). Carbon dioxide reforming of methane on nickel catalysts. *Chemical Engineering Science*, 44(12), 2825–2829, doi: 10.1016/0009-2509(89)85092-4

[28] Al-Doghachi, F.J., Zainal, Z., Saiman, M.I., Embong, Z., Taufiq-Yap, Y.H. (2015). Hydrogen production from dry-reforming of biogas over Pt/$Mg_{1-x}Ni_xO$ catalysts. *Energy Procedia*, 79, 18–25, doi: 10.1016/j.egypro.2015.11.460

[29] Kim, B.J., Jeon, K.W., Na, H.S., Lee, Y.L., Ahn, S.Y., Kim, K.J., Jang, W.J., Shim, J.O., Roh, H.S. (2020). Reducible oxide (CeO_2, ZrO_2, and CeO_2-ZrO_2) promoted Ni-MgO catalysts for carbon dioxide reforming of methane reaction. *Korean Journal of Chemical Engineering*, 37, 1130–1136, doi: 10.1007/s11814-020-0551-0

[30] Laosiripojana, N., Assabumrungrat, S. (2005). Catalytic dry reforming of methane over high surface area ceria. *Applied Catalysis B: Environmental*, 60(1–2), 107–116, doi: 10.1016/j.apcatb.2005.03.001

Copyright © 2021, ISSN 1978-2993

[31] Guo, J., Lou, H., Zhao, H., Chai, D., Zheng, X. (2004). Dry reforming of methane over nickel catalysts supported on magnesium aluminate spinels. *Applied Catalysis A: General*, 273(1–2), 75–82, doi: 10.1016/j.apcata.2004.06.014

[32] Atallah, E., Zeaiter, J., Ahmad, N., Kwapinska, M., Leahy, J. & Kwapinski, W. (2020). The effect of temperature, residence time, and water-sludge ratio on hydrothermal carbonization of DAF dairy sludge. *Journal of Environmental Chemical Engineering*, 8(1), 103599, doi: 10.1016/j.jece.2019.103599

[33] Kehres, J., Jakobsen, J. (2012). Dynamical Properties of a $Ru/MgAl_2O_4$ Catalyst during Reduction and Dry Methane Reforming. *J. Phys. Chem. C*, 116, 12407–21415, doi: 10.1021/jp3069656

[34] Topalidis, A., Petrakis, E., Ladavos, A., Loukatzikou, L., Pomonis, J. (2007). A kinetic study of methane and carbon dioxide interconversion over 0.5% $Pt/SrTiO_3$ catalysts. *Catalysis Today*, 127(1–4), 238–245, doi: 10.1016/j.cattod.2007.04.015

Copyright © 2021, ISSN 1978-2993